0090-9556/04/3210-1121–1131$20.00
DRUG METABOLISM AND DISPOSITION
DMD 32:1121–1131, 2004

Vol. 32, No. 10
315/1174736
Printed in U.S.A.

ROLE OF ITRACONAZOLE METABOLITES IN CYP3A4 INHIBITION

Nina Isoherranen, Kent L. Kunze, Kyle E. Allen, Wendel L. Nelson, and Kenneth E. Thummel

Department of Pharmaceutics (N.I., K.E.T.) and Department of Medicinal Chemistry (K.L.K., K.E.A., W.L.N.), University of Washington, Seattle US.

Received April 19, 2004; accepted July 6, 2004

ABSTRACT:

Itraconazole (ITZ) is a potent inhibitor of CYP3A in vivo. However, unbound plasma concentrations of ITZ are much lower than its reported in vitro K_i, and no clinically significant interactions would be expected based on a reversible mechanism of inhibition. The purpose of this study was to evaluate the reasons for the in vitro-in vivo discrepancy. The metabolism of ITZ by CYP3A4 was studied. Three metabolites were detected: hydroxy-itraconazole (OH-ITZ), a known in vivo metabolite of ITZ, and two new metabolites: keto-itraconazole (keto-ITZ) and *N*-desalkyl-itraconazole (ND-ITZ). OH-ITZ and keto-ITZ were also substrates of CYP3A4. Using a substrate depletion kinetic approach for parameter determination, ITZ exhibited an unbound K_m of 3.9 nM and an intrinsic clearance (CL_{int}) of 69.3 ml · min^{-1} · nmol CYP3A4^{-1}. The respective unbound K_m values for OH-ITZ and keto-ITZ were 27 nM and 1.4 nM and the CL_{int} values were 19.8 and 62.5 ml · min^{-1} · nmol CYP3A4^{-1}. Inhibition of CYP3A4 by ITZ, OH-ITZ, keto-ITZ, and ND-ITZ was evaluated using hydroxylation of midazolam as a probe reaction. Both ITZ and OH-ITZ were competitive inhibitors of CYP3A4, with unbound K_i (1.3 nM for ITZ and 14.4 nM for OH-ITZ) close to their respective K_m. ITZ, OH-ITZ, keto-ITZ and ND-ITZ exhibited unbound IC_{50} values of 6.1 nM, 4.6 nM, 7.0 nM, and 0.4 nM, respectively, when coincubated with human liver microsomes and midazolam (substrate concentration < K_m). These findings demonstrate that ITZ metabolites are as potent as or more potent CYP3A4 inhibitors than ITZ itself, and thus may contribute to the inhibition of CYP3A4 observed in vivo after ITZ dosing.

Itraconazole (ITZ; Fig. 1) is a widely used triazole antifungal agent. It has a broad spectrum of activity and is effective against many fluconazole-resistant strains of fungi (Haria et al., 1996). In humans, the pharmacokinetic behavior of ITZ is characterized by intermediate bioavailability (55%), low-intermediate clearance (23 l/h), extensive tissue distribution, and a large apparent volume of distribution (11 l/kg) (Heykants et al., 1989; Poirier and Cheymol, 1998). Itraconazole is mainly eliminated from the body via metabolism, and more than 30 different metabolites have been proposed (Heykants et al., 1989; Poirier and Cheymol, 1998). Only one of these metabolites has been studied in humans, hydroxy-itraconazole (OH-ITZ; Fig. 1). Hydroxy-itraconazole possesses antifungal activity similar to that of ITZ, and it circulates in plasma at higher concentrations than does ITZ (Heykants et al., 1989; Poirier and Cheymol, 1998). At present, it is not known which P450 enzymes contribute to OH-ITZ formation in vivo or in vitro.

The steady-state concentrations of ITZ cannot be predicted from single-dose data (Poirier and Cheymol, 1998), and multiple-dose administration results in a 26 to 60% increase in elimination half-life and a 69 to 80% reduction in oral clearance of ITZ (Hardin et al., 1988). In addition, ITZ exhibits disproportional increases in AUC with increasing single oral doses (Heykants et al., 1989; Haria et al., 1996) and dose-dependent bioavailability (Schäfer-Körting, 1993). These findings suggest that metabolism of ITZ may be saturable at clinically relevant plasma concentrations or that one of the metabolites of ITZ inhibits its metabolism. Clinical evidence suggests that ITZ is mainly eliminated by CYP3A. Phenytoin, a known inducer of CYP3A4, caused a 17-fold increase in ITZ oral clearance (Ducharme et al., 1995). Administration of other CYP3A4 inducers, such as rifampicin (Tucker et al., 1992), carbamazepine, and phenobarbital (Bonay et al., 1993), result in undetectable ITZ plasma concentrations, probably due to increased first-pass extraction as well as faster systemic elimination.

The evidence for involvement of CYP3A in ITZ elimination in vivo together with the nonlinear kinetics of ITZ are consistent with well established inhibition interactions between ITZ and other CYP3A substrates. Drugs whose pharmacokinetics is significantly affected by ITZ include cyclosporine (Kwan et al., 1987; Trenk et al., 1987; Florea et al., 2003), tacrolimus (Banerjee et al., 2001; Mahnke et al., 2003), midazolam (Olkkola et al., 1996; Backman et al., 1998), buspirone (Kivistö et al., 1999), methylprednisolone (Lebrun-Vignes et al., 2001), lovastatin (Neuvonen and Jalava, 1996), and simvastatin (Neuvonen et al., 1998). The observed increase in the in vivo AUC of these drugs is between 2- and 30-fold after concomitant administration of ITZ.

ITZ is a relatively potent inhibitor of CYP3A4 in vitro. However, K_i values determined in vitro for CYP3A4 range from 27 nM to 11 μM (Back and Tjia, 1991; von Moltke et al., 1996; Wang et al., 1999;

This study was supported in part by National Institutes of Health Grant P01 GM32165.

Article, publication date, and citation information can be found at http://dmd.aspetjournals.org.

doi:10.1124/dmd.104.000315.

ABBREVIATIONS: ITZ, itraconazole; OH-ITZ, hydroxy-itraconazole; keto-ITZ, keto-itraconazole; ND-ITZ, *N*-desalkyl-itraconazole; OH-MDZ, 1′-hydroxymidazolam; HLM, human liver microsome; HPLC, high performance liquid chromatography; KPi, monobasic phosphate; MS/MS, tandem mass spectrometry; LC-MS, liquid chromatography-mass spectrometry; P450, cytochrome P450, K_m, Michaelis constant; K_i, inhibition constant, CL_{int}, intrinsic clearance; AUC, area under the curve.

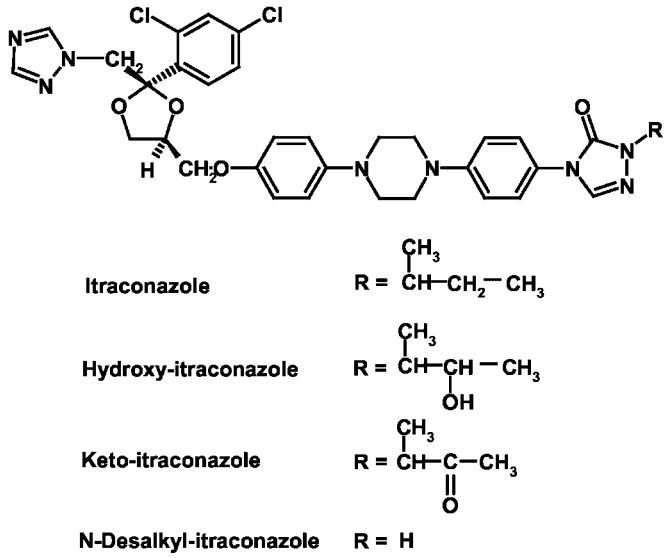

FIG. 1. Chemical structures of ITZ, OH-ITZ, keto-ITZ, and ND-ITZ.

Ishigam et al., 2001). Differences in experimental microsomal protein content (0.04–0.25 mg/ml) and nonspecific binding of ITZ to microsomal protein may account for this large variation in observed K_i values. Despite the relatively high affinity of ITZ for CYP3A4, its unbound plasma concentrations are generally lower (1–3 nM) than the lowest reported K_i. Assuming a reversible inhibition mechanism, a ratio of unbound ITZ concentration to K_i less than 1 suggests that no clinically significant interaction involving CYP3A should occur. However, this is clearly inconsistent with the observed in vivo interactions described above.

Concentrative uptake of ITZ into hepatocytes might account for the apparent in vitro-in vivo discrepancy described above. In this regard, Yamano et al. (2001) reported that, in the rat, the unbound hepatic concentration of ITZ can greatly exceed (11- to 14-fold) the unbound plasma concentration (Yamano et al., 2001). Although active uptake of ITZ into human hepatocytes may also occur, we considered an alternative hypothesis, formation of CYP3A-inhibitory metabolites, that could contribute to the apparent in vitro-in vivo discrepancy.

Thus, the goals of this study were to 1) determine whether CYP3A4/5 catalyze the initial oxidations of ITZ and 2) evaluate whether the discrepancy between in vitro and in vivo data with respect to inhibition of CYP3A4 by ITZ is due to a failure to account for in vivo inhibitory ITZ metabolites, extensive nonspecific binding of ITZ to microsomal proteins in vitro, or rapid depletion of ITZ in vitro. To address these aims, the sequential metabolism of ITZ by CYP3A4 was studied using human liver microsomes and heterologously expressed CYP3A4 (Supersomes). Three metabolites formed by CYP3A4 were identified. The inhibitory potencies of ITZ and its identified metabolites toward CYP3A4 were determined, and their unbound concentrations in microsomal incubations were measured to obtain unbound IC_{50} values for comparison.

Materials and Methods

Chemicals. Itraconazole and hydroxy-itraconazole were purchased from Research Diagnostics (Flanders, NJ). Keto-itraconazole was generously provided by Dr. Jan Heeres (Janssen Pharmaceuticals, Beerse, Belgium). The metabolite was also prepared in our laboratory by Swern oxidation from hydroxy-itraconazole (Tidwell, 1990; Weerawarna et al., 1991). *N*-Desalkyl-itraconazole was prepared from an intermediate hydrazide-carboxamide, also provided by Dr. Heeres, by reaction with formamidine acetate to generate the triazolone ring, as previously reported (Heeres et al., 1984). Midazolam, 1′-hydroxymidazolam (OH-MDZ), and 1′-[$^2H_2$]-hydroxymidazolam were gifts from Hoffman-La Roche (Nutley, NJ). Acetonitrile was purchased from Fisher Chemicals (Fairlawn, NJ), ammonium acetate from J.T. Baker (Phillipsburg, NJ), and NADPH from Sigma-Aldrich (St. Louis, MO). Ultrapure water, filtered through a Barnstead Nanopure filter system, was used throughout the study.

Human Liver Microsomes (HLMs) and Recombinant P450s. HLMs were prepared by a standard ultracentrifugation technique from five donor livers selected from the University of Washington Human Liver Bank (Lin et al., 2002). All were known to be devoid of significant amounts of CYP3A5 protein (*CYP3A5*3/*3* genotype). The protein concentration in each HLM was measured by standard methods (Lowry et al., 1951). Equal amounts of microsomal protein from the five different preparations were pooled for subsequent experimentation. Supersomes containing cDNA-expressed CYP3A4 coexpressed with P450-reductase (oxidoreductase) and cytochrome b_5 were purchased from BD Gentest (Woburn, MA). Additional Supersomes containing cDNA-expressed P450-reductases and P450s 1A1, 1A2, 2A6 (with b_5), 2B6 (with b_5), 2E1 (with b_5), 2C9 (with b_5), 2C19 (with b_5), 2D6, and 3A5 were also purchased from BD Gentest.

Identification of ITZ Metabolites Formed by CYP3A4. ITZ metabolites were identified primarily by mass spectrometry and by comparing the HPLC retention times of metabolite peaks to available reference compounds. ITZ or one of its metabolites [OH-ITZ or keto-itraconazole (keto-ITZ)] was incubated at 1 μM concentration with 100 pmol of CYP3A4 Supersomes in 0.5 ml of 100 mM monobasic phosphate buffer (KPi), pH 7.4, with 1 mM EDTA and with or without NADPH (1 mM) for 60 min at 37°C. At the end of the incubation, the reaction was terminated by the addition of 5 ml of dichloromethane. The organic phase was separated and evaporated to dryness under a nitrogen stream and the sample residue reconstituted in 200 μl of acetonitrile. Twenty microliters of the solution were injected into the Hewlett Packard (Palo Alto, CA) series 1100 MSD system, and analytes were eluted according to the method used for quantitation of metabolites (see section below). Total ion monitoring was conducted to obtain information about molecular weight (quasimolecular ions) and chloride isotope patterns together with the retention time of the metabolite.

For additional structural information, MS/MS analysis of the quasimolecular ion was conducted for ITZ and its three identified metabolites, OH-ITZ, keto-ITZ, and *N*-desalkyl-itraconazole (ND-ITZ). The MS/MS spectra were recorded using a Micromass Quattro II triple quadrupole mass spectrometer (Waters, Milford, MA) operated on the positive ion electrospray atmospheric pressure ionization mode. The mass spectrometer was equipped with a Shimadzu LC-10AD pump, DGU-14A degasser, SCL-10A controller, SIL-10AD autosampler, and Micromass Masslynx data analysis software. For the MS, the cone voltage was 30 V and the collision energy with argon 35 eV. Capillary voltage was 3.5 kV, source temperature 150°C, and desolvation temperature 350°C; the drying gas was set at 400 and nebulizing gas at 25. The scan time was 2.5 s and interscan time 0.1 s. The fragments produced from ions with *m/z* 705 (ITZ), *m/z* 721 (OH-ITZ), *m/z* 719 (keto-ITZ), and *m/z* 649 (ND-ITZ) were recorded in separate chromatographic runs. The compounds were separated by HPLC using a Zorbax Eclipse XDB-C8 5-μm column (2.1 mm i.d. × 50 mm; Agilent Technologies, Palo Alto, CA). The mobile phase flow was 0.2 ml/min and the following gradient was used. The initial conditions of 40% aqueous (5 mM ammonium acetate buffer, pH 6.8) and 60% acetonitrile were held for half a minute after injection, after which the acetonitrile concentration was increased linearly to 70% over 1.5 min and further to 80% over 2 min. The acetonitrile concentration was then increased linearly over 1.5 min to 95% and held at 95% for 0.5 min.

Incubation Conditions for Substrate Depletion Experiments. All substrates (ITZ, OH-ITZ, and keto-ITZ) were dissolved in acetone and added to the incubations at appropriate concentrations that gave a final acetone concentration in the incubation of 1%. The incubations were performed in 100 mM KPi buffer (pH 7.4) with 1 mM EDTA. The NADPH concentration in all incubations was 1 mM. Insect cell-expressed CYP3A4 Supersomes (coexpressed with P450 reductase and cytochrome b_5) were used in all incubations at a concentration of 10 pmol of CYP3A4/ml (0.084 mg of microsomal protein/ml). Pilot incubation experiments were performed with human liver microsomes and heterologously expressed CYP3A4 Supersomes to determine steady-state conditions (protein and time linearity) and to identify potential

metabolites of ITZ formed by CYP3A4. Significant and rapid substrate depletion was observed for ITZ and its metabolites. Therefore, a substrate depletion approach was adopted for determination of kinetic parameters.

For substrate depletion studies, all incubations were performed in duplicate. A starting incubation volume of 1.4 ml was used. After preincubation for 4 min at 37°C, a time 0 min sample (200 μl) was transferred to a vial containing 200 μl of ice-cold acetonitrile and the reaction was initiated with NADPH (final concentration 1 mM). At time points 1, 2, 5, 10, and 15 min, 200-μl samples were transferred to tubes containing 200 μl of ice-cold acetonitrile for quenching the reaction. The samples were vortexed and centrifuged at 12,000*g* for 10 min, and the supernatant was transferred to an HPLC vial for liquid chromatography-mass spectrometry (LC-MS) analysis.

Incubation Conditions for Incubation of P450 Panel with ITZ. Formation of OH-ITZ from ITZ by CYP1A1, CYP1A2, CYP2A6, CYP2B6, CYP2C9, CYP2C19, CYP2D6, CYP2E1, CYP3A4, and CYP3A5 was tested using heterologously expressed P450 Supersomes obtained from BD Gentest. Each incubation was performed in 200 μl of 100 mM KPi buffer, pH 7.4, with 50 pmol of the respective P450 isoform. The final ITZ concentration was 500 nM. The metabolic reactions were initiated with the addition of NADPH (1 mM) and allowed to proceed for 10 min. After 10 min, the reactions were quenched with the addition of 200 μl of acetonitrile, and formation of OH-ITZ, keto-ITZ, and ND-ITZ was measured by LC-MS. CYP3A5-catalyzed formation of OH-ITZ from ITZ (50 nM and 1 μM) with and without additional cytochrome b_5 was also examined. Additionally, depletion of ITZ by CYP3A4 and CYP3A5 (with and without supplemented b_5) was tested at ITZ concentrations of 50 nM and 500 nM. For these experiments, ITZ was incubated with the enzyme for 30 min and samples were collected at 5, 15, and 30 min after initiation of metabolism by NADPH.

Quantitation of ITZ, OH-ITZ, keto-ITZ, and ND-ITZ by LC-MS. ITZ, OH-ITZ, keto-ITZ, and ND-ITZ concentrations were measured by high performance LC-MS using a Hewlett Packard series 1100 MSD system operating in the positive ion electrospray mode with selected ion monitoring and equipped with HP Chemstation data analysis software. The mobile phase consisted of acetonitrile and 5 mM ammonium acetate buffer (pH 7.0) with a gradient elution. Twenty microliters of the sample were injected onto the column. The mobile phase flow was 0.25 ml/min and the initial mobile phase was 40% acetonitrile and 60% 5 mM ammonium acetate buffer. The acetonitrile concentration was increased linearly to 70% over 3 min and then to 85% over 1 min and finally to 95% over 1 min. After 0.5 min, the acetonitrile concentration was decreased back to 40%. Analyte separation was achieved using a Zorbax Eclipse XDB-C8 5-μm column (2.1 mm i.d. $\times$ 50 mm; Agilent Technologies) equipped with a Phenomenex C8 guard column (2.1 mm i.d $\times$ 4 mm). Ion *m*/*z* 705 was monitored for ITZ, *m*/*z* 721 for OH-ITZ, *m*/*z* 719 for keto-ITZ, and *m*/*z* 649 for ND-ITZ. For the mass spectrometer, the drying gas flow was set at 10 l/min, nebulizer pressure at 25 psig, gas temperature at 300°C, and capillary voltage (V_{cap}) at 5500 V. The fragmentor was set at 85 V for all ions.

Calibration curves for ITZ, OH-ITZ, and keto-ITZ were prepared between the concentrations 1 nM and 1000 nM. For ND-ITZ, the calibration curve was between 1 nM and 500 nM. The limit of detection for ITZ and its metabolites was 1 nM and the limit of quantification 5 nM. At a 50 nM nominal concentration, the accuracy for ITZ measurement was 99.2%, and the precision ($n = 6$), measured as %CV, was 7.6%. For OH-ITZ measurements, the accuracy at a 50 nM nominal concentration was 100.5%, and the precision ($n = 6$) was 5.0%. The accuracy of keto-ITZ measurement at 50 nM was 102.4% and the precision was 7.4% ($n = 6$).

Nonspecific Binding of ITZ, OH-ITZ, keto-ITZ, and ND-ITZ in Human Liver Microsomes and Supersomes. The nonspecific protein binding of ITZ, OH-ITZ, keto-ITZ, and ND-ITZ was studied using the tube absorption method described by Ishigam et al. (2001). The method utilizes the propensity of basic lipophilic drugs to adsorb to experimental materials such as the inner wall of an incubation tube. The concentrations of the test compounds were measured by the same LC-MS method as described for microsomal incubations. Two sets of solutions, one with microsomal protein and one without microsomal protein, were prepared. To these, solutions of ITZ, OH-ITZ, keto-ITZ, or ND-ITZ in acetone were added to achieve a final volume of 300 μl (a samples) or 200 μl (b samples) of 100 mM KPi buffer (1 mM EDTA, pH 7.4). The final acetone concentration was fixed at 1%. For Supersomes, ITZ and OH-ITZ were added at nominal concentrations of 25, 50, 250, 500, and 1000 nM. For liver microsomes, all compounds were added to produce a nominal concentration of 50, 250, and 500 nM. The protein concentrations were either 10 pmol of CYP3A4/ml (0.085 mg of protein/ml) of Supersomes or 0.025 mg/ml for pooled (five livers selected for the study) HLMs. The solutions were vortexed and incubated at 37°C for 60 min. After the 60-min incubation, either a 200-μl aliquot was transferred to another tube containing 200 μl of acetonitrile (sample a) or 200 μl of acetonitrile were added into a tube containing the test compound in 200 μl of KPi buffer (sample b). All samples were mixed and centrifuged (12,000*g*, 10 min), and the supernatant fraction was transferred to an autosampler vial and analyzed by LC-MS. From the a samples, the concentration not adsorbed to the tube wall (C_u for samples containing only buffer and drug and C_m for samples containing microsomal protein) was measured. From the b samples, the total drug concentrations in the tube were measured [C_t for buffer samples and $C_{t(m)}$ for microsomal or supersomal samples]. The drug concentration adsorbed to the tube wall (C_w) was calculated from the buffer-containing samples as follows:

$$C_w = C_t - C_u \quad (1)$$

The ratio of the unbound concentration to that adsorbed to the wall (*r*; partitioning constant for the wall) was calculated from the quotient of C_u and C_w. The concentration adsorbed to the tube wall when the drug was mixed with microsomes or Supersomes was calculated as:

$$C_{w(m)} = C_{t(m)} - C_m \quad (2)$$

The unbound concentrations in microsomal suspension [$C_{u(m)}$] were calculated from:

$$C_{u(m)} = r_{mean} \cdot C_{w(m)} \quad (3)$$

in which r_{mean} represents the mean value of *r* obtained at varying substrate concentrations. The *r* value was found to be independent of substrate concentration over the range of interest. The unbound fraction for microsomes [$f_{u(m)}$] was calculated using the equation:

$$f_{u(m)} = \frac{C_{u(m)}}{C_m} \quad (4)$$

All measurements were conducted in triplicate.

Inhibition of CYP3A4 in Human Liver Microsomes and Supersomes by ITZ and Its Metabolites. *Microsomal experiments.* The IC_{50} value for ITZ, OH-ITZ, keto-ITZ, and ND-ITZ in human liver microsomes was measured using 1′-hydroxylation of midazolam (OH-MDZ) as a probe reaction for CYP3A4-mediated metabolism. All the human liver microsomes used were known not to express appreciable levels of CYP3A5. The incubations were performed in 100 mM KPi buffer (pH 7.4) with 1 mM EDTA. The NADPH concentration in all incubations was 1 mM. Pooled human liver microsomes were used with a final protein concentration of 0.025 mg/ml. The midazolam concentration was 1 μM in all incubations. ITZ, OH-ITZ, and keto-ITZ were added to the 500-μl incubations at nominal concentrations of 0, 5, 25, 50, 100, 250, 500, and 1000 nM. After preincubation for 4 min at 37°C, a time 0 min sample (200 μl) was collected into a vial containing 200 μl of acetonitrile, and the reaction was initiated with NADPH (final concentration 1 mM) and allowed to proceed for 2 min. At 2 min, another 200-μl sample was taken and the reaction quenched with 200 μl of ice-cold acetonitrile. Ten microliters of internal standard solution (D_2-labeled OH-MDZ, 100 ng/ml) were added. All incubations were carried out in duplicate. The inhibitor concentration was measured at time 0 min and at time 2 min, and the mean inhibitor concentration was calculated for the incubation period (i.e., the inhibitor concentration was corrected for depletion). OH-MDZ was measured only in the 2-min sample.

OH-MDZ concentrations were measured using a Hewlett Packard series 1100 MSD system operating at the positive ion electrospray mode with selected ion monitoring. The mobile phase consisted of methanol and water, both with 0.1% acetic acid, with a gradient elution. Twenty microliters of the sample were injected into the HPLC apparatus. The mobile phase flow was 0.25 ml/min and the initial mobile phase was 45% methanol and 65% water. The methanol concentration was increased linearly to 60% over 2 min. After 0.5 min, the methanol concentration was increased to 90% over 1.5 min and

kept there for 1 min. At 5 min, the methanol concentration was decreased back to 45%. Separation was achieved using a Zorbax Eclipse XDB-C8 5-μm column (2.1 mm i.d. $\times$ 50 mm; Agilent Technologies) equipped with a Phenomenex SecurityGuard C8 guard column. Ion *m/z* 342 was monitored for OH-MDZ and *m/z* 346 for the D_2-labeled OH-MDZ (^{37}Cl-isotope). For the mass spectrometer, the drying gas flow was 10 l/min, nebulizer pressure 25 psig, gas temperature 300°C, and capillary voltage (V_{cap}) 5000 V. The fragmentor was set at 110 V for all ions. The OH-MDZ calibration curve was prepared over a concentration range (10 different concentrations) between 1.2 and 350 ng/ml. The limit of quantification for OH-MDZ was 1.2 ng/ml. At mid-concentration (50 ng/ml), the accuracy of the OH-MDZ measurement was 101.8%, and the precision of the assay was 8.9%.

Supersome experiments. The inhibition constant (K_i) for ITZ and OH-ITZ was determined using heterologously expressed CYP3A4 (Supersomes). The incubation mixture consisted of 5 pmol (10 pmol/ml) of cDNA-expressed CYP3A4 (0.084 mg/ml of total microsomal protein), midazolam (at concentrations of 1, 2, 4, and 8 μM), and either ITZ or OH-ITZ (at nominal concentrations of 0, 50, 100, 500, and 1000 nM) in 500 μl of 100 mM KPi buffer (pH 7.4) with 1 mM EDTA. After preincubation for 4 min at 37°C, a time 0 min sample (200 μl) was collected into a vial containing 200 μl of acetonitrile, and the reaction was initiated with NADPH (1 mM final concentration) and allowed to proceed for 2 min. At 2 min, another 200-μl sample was taken and quenched into 200 μl of ice-cold acetonitrile, and 10 μl of internal standard solution (D_2-OH-MDZ, 100 ng/ml) were added. All incubations were carried out in duplicate. The acetonitrile-quenched samples were analyzed using the LC-MS methods described above for ITZ, OH-ITZ, and keto-ITZ in both the 0-min and 2-min samples, whereas OH-MDZ was quantified only from the 2-min samples. The inhibitor concentrations in all incubations were again corrected for inhibitor depletion.

Calculation of Enzyme Kinetic Parameters. The Michaelis constant (K_m) was determined by the method described by Obach and Reed-Hagen (2002). A first-order decay function was fit to the data from the logarithm of the percentage of the substrate remaining versus time at each substrate concentration to determine initial substrate depletion rate constants (k_{dep}). This parameter is equivalent to the apparent clearance ($v/[S]$) of the drug at any given concentration. Only the initial time points, wherein log-linearity was observed, were used to determine depletion rate constants. K_m values were determined from the expanded Michaelis-Menten equation by fitting the k_{dep} versus the substrate concentration on a linear-log plot to the equation

$$k_{dep} = k_{dep[S]\to 0} \cdot \left(1 - \frac{[S]}{[S] + K_m}\right) \quad (5)$$

in which $[S]$ is the substrate concentration, $k_{dep[S]\to 0}$ represents the theoretical maximum substrate consumption rate under the experimental conditions and K_m is the Michaelis constant (SigmaPlot; SPSS Inc., Chicago, IL).

The intrinsic clearance (CL_{int}) of each substrate was determined from the maximum depletion rate constant ($k_{dep[S]\to 0}$) by dividing this value by the enzyme concentration in the incubation:

$$CL_{int,u} = \frac{k_{dep[s]\to 0}}{C_{CYP3A4}} \quad (6)$$

The maximal substrate consumption velocity, V_{max}, was obtained using the relationship between CL_{int}, $CL_{int,u}$, K_m, and V_{max}:

$$V_{max} = CL_{int,u} \cdot K_m \quad (7)$$

For this approach the unbound K_m was used and the $CL_{int,u}$ was calculated as described by eq. 6.

The inhibition parameters were determined by use of nonlinear regression analysis. A standard competitive and noncompetitive inhibition model was fit to the experimental data (Systat 5.04; Systat Software Inc., Point Richmond, CA).

Results

Identification of ITZ Metabolites Formed by CYP3A4. The first goal of this study was to confirm that ITZ is a substrate for CYP3A in vitro and to characterize the metabolites generated. In preliminary studies with heterologously expressed CYP3A4, it was found that CYP3A4 metabolized ITZ efficiently to the primary metabolite OH-ITZ. An unknown metabolite with *m/z* 719 [MH^+] was detected from the same ITZ-CYP3A4 incubations. MH^+ ions corresponding to a chlorine isotope pattern with two chlorine atoms were observed at *m/z* 719 and *m/z* 721. Based on the molecular weight, MS-MS fragmentation pattern (see Fig. 3), and comparison of retention times (Fig. 2) and MS spectrum of the produced metabolite to a synthetic reference material, this unknown metabolite produced by CYP3A4 was identified as the corresponding ketone of OH-ITZ (keto-ITZ; Fig. 1). Incubation of this new metabolite showed that it too was a substrate of CYP3A4, and efforts were made to identify additional downstream metabolites. A product with a shorter retention time than OH-ITZ (Fig. 2) and MH^+ ions at *m/z* 649 and *m/z* 651 corresponding to the

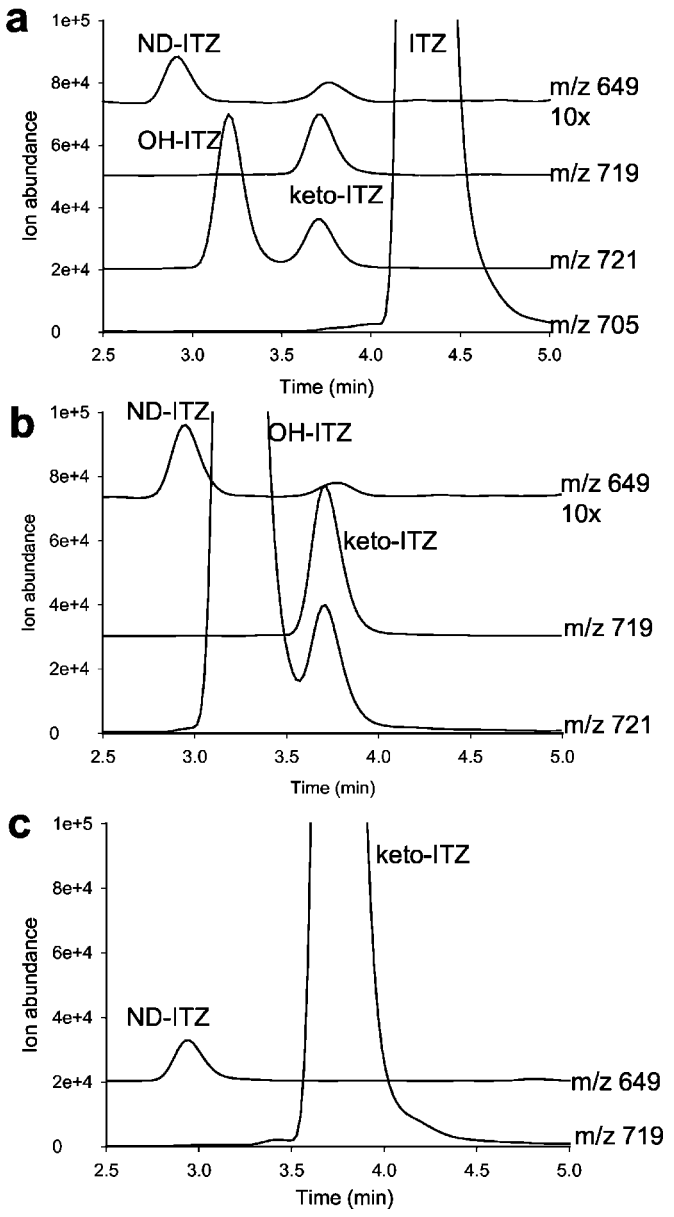

FIG. 2. Selected mass spectrometric ion chromatograms from incubations of ITZ (a), OH-ITZ (b), and keto-itraconazole (c) with heterologously expressed CYP3A4. Identified peaks were ITZ, OH-ITZ, keto-ITZ, and ND-ITZ. In a and b, an ND-ITZ ion chromatogram is expanded 10-fold. Substrate concentrations in incubations were 1000 nM, and incubation conditions were as described under *Materials and Methods*.

Cl isotope pattern of the molecule was detected. The confirmation for the MH^+ ions at *m/z* 649 and *m/z* 651 was obtained from detection of sodium and potassium adducts (*m/z* 671, 673, and *m/z* 687 and 689, respectively) and a M^{2+} ion at *m/z* 325. Based on a comparison to the synthetic reference material, this metabolite was identified as *N*-desalkyl-itraconazole (ND-ITZ; Fig. 1). This metabolite was also detected in incubations of ITZ and OH-ITZ with CYP3A4 (Fig. 2). MS/MS characterization of the metabolically produced compound further confirmed the structure (Fig. 3).

Qualitatively, based on the metabolite identification data, a sequential metabolic pathway for ITZ with CYP3A4 was established (Fig. 4). In this metabolic pathway, ITZ first undergoes hydroxylation to OH-ITZ and then a second oxidation to keto-ITZ. keto-ITZ is further oxidized to undergo *N*-dealkylation to ND-ITZ. Because ND-ITZ was measured also in incubations with ITZ and OH-ITZ at saturating substrate concentrations, the possibility that *N*-dealkylation occurs directly from ITZ and/or from OH-ITZ cannot be excluded.

Only CYP3A4 and CYP1A1 catalyzed the metabolism of ITZ to OH-ITZ. In addition, none of the P450 isoforms, except CYP3A4, generated keto-ITZ or ND-ITZ. With respect to CYP1A1 and OH-ITZ formation, the rate of metabolism (500 nM, nominal concentration) was approximately 3 pmol · min^{-1} · $nmol^{-1}$ 1A1, and no significant

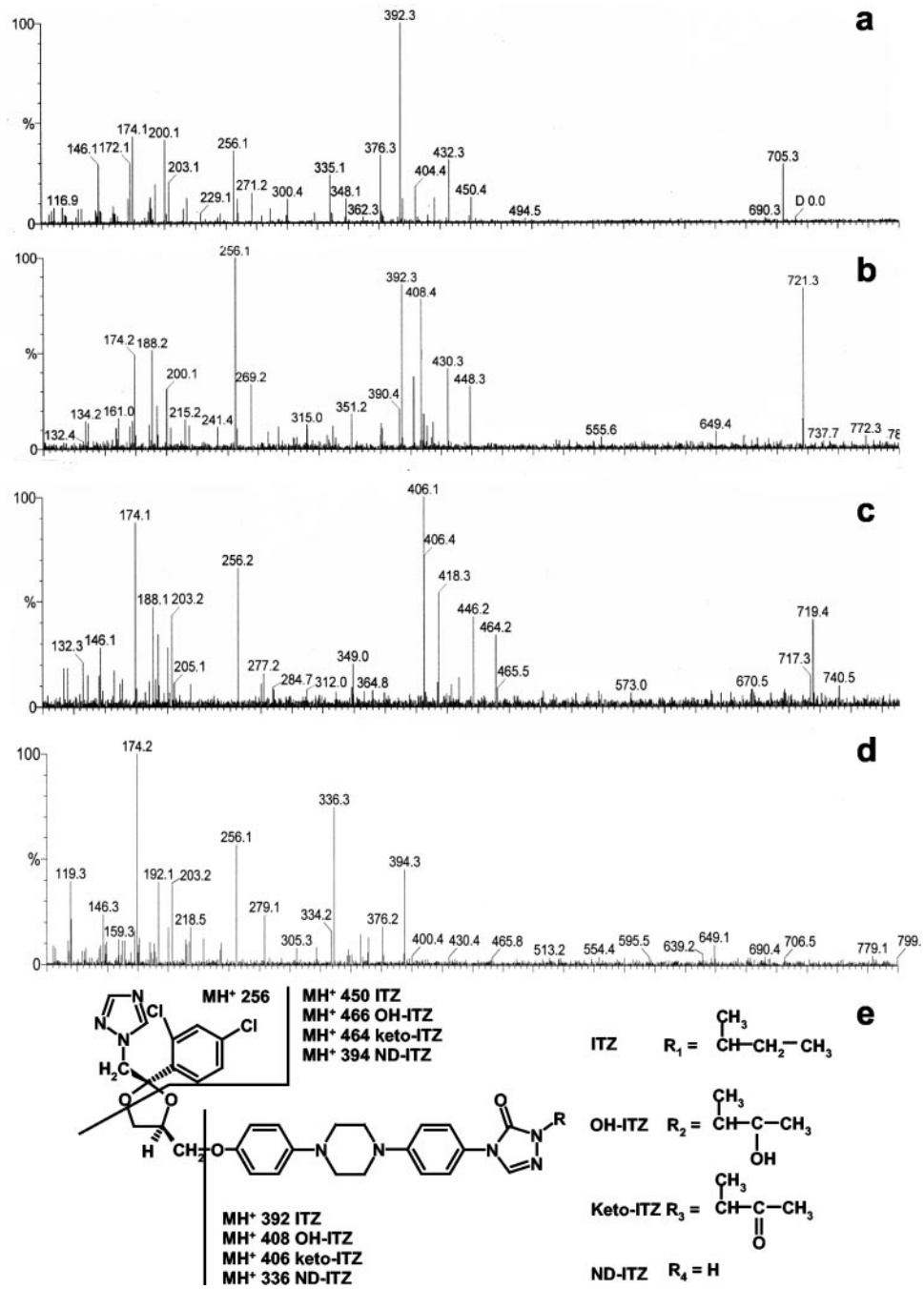

FIG. 3. MS/MS characterization of ITZ metabolites. MS/MS spectra of ITZ standard using ion *m/z* 705 (a), OH-ITZ standard using ion *m/z* 721 (b), metabolically produced keto-ITZ using ion *m/z* 719 (c), metabolically produced ND-ITZ using ion *m/z* 649 (d), and suggested fragmentation pattern for ITZ, OH-ITZ, keto-ITZ, and ND-ITZ (e). Incubation conditions for generating keto-ITZ and ND-ITZ were as described under *Materials and Methods*. ITZ and OH-ITZ spectra were obtained from a control incubation in which no NADPH was added.

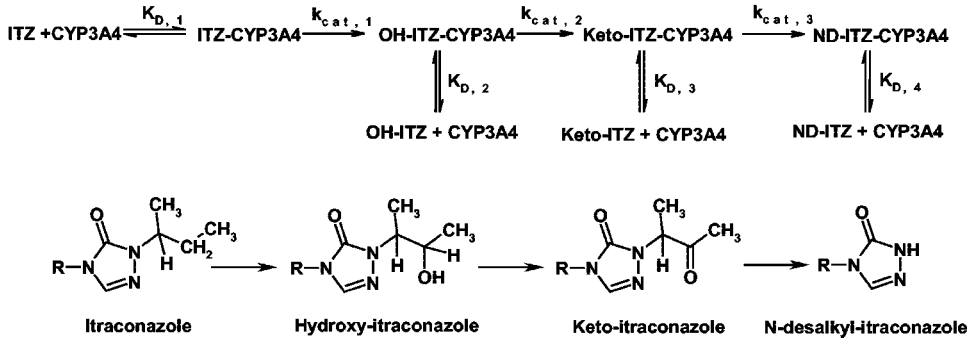

FIG. 4. Suggested sequential CYP3A4-catalyzed metabolic pathway for ITZ. Rate constants for metabolism (k_{cat}) and release of ITZ and metabolite intermediates (K_D) are included to illustrate the possibility for nondissociative or dissociative sequential metabolism.

substrate depletion was observed. The combined formation velocity for OH-ITZ and keto-ITZ catalyzed by CYP3A4 was approximately 15 pmol · min^{-1} · $nmol^{-1}$ 3A4, but in this experiment, significant depletion of ITZ was observed (>50%), which may have masked the true reaction velocity.

It was of interest to note that CYP3A5 (with or without cytochrome b_5 supplementation) did not catalyze OH-ITZ formation, nor was there any evidence of significant metabolism to alternative products, as indicated by a flat substrate disappearance curve over 30 min of incubation. This was in marked contrast to a 44% and 20% depletion of ITZ at concentrations 50 nM and 500 nM, respectively, when it was incubated with CYP3A4 under the same conditions.

Kinetic Analysis of ITZ Metabolism. The enzyme kinetic parameters for ITZ metabolism were estimated using a substrate depletion approach. This method was adopted because ITZ appears to undergo sequential metabolism to multiple metabolites, and significant substrate depletion was observed even at incubation times of 1 to 2 min. Figure 5, a and b, shows the concentration versus time profiles for ITZ, OH-ITZ, and keto-ITZ after incubation of 28 and 580 nM ITZ with CYP3A4. An early rapid depletion of ITZ was accompanied by the appearance of OH-ITZ and keto-ITZ. ND-ITZ concentrations in these incubations were below the limits of quantification. At the lower ITZ concentrations, the concentration of OH-ITZ and keto-ITZ appeared to reach a maximum and subsequently declined with time, indicating that the two metabolites were also substrates of CYP3A4. Moreover, at the lowest ITZ concentration, there was a failure to achieve mass-balance with an accounting of the detectable metabolites, suggesting that further biotransformation occurred.

To evaluate further the sequential metabolism of ITZ, substrate depletion experiments with OH-ITZ (Fig. 5, c and d) and keto-ITZ (Fig. 5, e and f) were performed. keto-ITZ and ND-ITZ appeared to be primary metabolites of OH-ITZ and keto-ITZ, respectively. At the lowest substrate (OH-ITZ) concentrations tested, the concentration of keto-ITZ rose to a maximum and declined thereafter over time, and mass-balance was again not achieved. The concentrations of ND-ITZ in incubations of ITZ and OH-ITZ were not measurable (below the limit of quantification). In incubations with keto-ITZ, ND-ITZ could be quantified, but mass-balance was not obtained (Fig. 5, e and f). In incubations of ITZ and OH-ITZ with high enzyme (CYP3A4) concentrations (100 pmol/ml), ND-ITZ was also quantifiable. Preliminary experiments incubating ND-ITZ with CYP3A4 showed that it is also further depleted by CYP3A4 (data not shown).

For all three substrates (ITZ, OH-ITZ, and keto-ITZ), biphasic depletion curves were observed (not shown). This biphasic behavior was most pronounced at the lowest substrate concentrations. For kinetic parameter estimation, only the initial log-linear portion of the depletion curve was used. A simple hyperbolic equation (eq. 5) was fit to the substrate depletion data to obtain the Michaelis constants (K_m) and the theoretical maximum depletion rate constants (k_{dep}^{max}) for ITZ, OH-ITZ, and keto-ITZ with CYP3A4. A summary of the resulting parameters is presented in Table 1. The relationship between the first-order rate constant for substrate depletion (k_{dep}) and the substrate concentration [S] for each of the compounds is shown in Fig. 6. All three molecules had similar unbound K_m values at the low nanomolar range, showing that ITZ, OH-ITZ, and keto-ITZ all have a high affinity to CYP3A4. The turnover rates of ITZ, OH-ITZ, and keto-ITZ were relatively slow, <1 min^{-1}, consistent with a "high affinity-low capacity" classification. Interestingly, OH-ITZ had the lowest unbound intrinsic clearance of the studied compounds, and it is known to accumulate to levels above that of ITZ in vivo.

Inhibition of CYP3A4 by ITZ, OH-ITZ, and keto-ITZ. The inhibition constants for ITZ and OH-ITZ were measured using CYP3A4 Supersomes and midazolam as a probe substrate. Figure 7 shows the Lineweaver-Burk and Dixon plots for inhibition of OH-MDZ formation by ITZ and OH-ITZ. Inspection of the reciprocal plots suggests that ITZ and OH-ITZ are competitive inhibitors of CYP3A4. This suggestion was confirmed by nonlinear regression analysis using alternative models. For ITZ, a small but insignificant noncompetitive component was detected, as well, using nonlinear regression. The kinetic parameters for CYP3A4 inhibition are summarized in Table 2. Both ITZ and OH-ITZ appeared to be high-affinity inhibitors of CYP3A4, based on the low nanomolar unbound K_i.

In incubations of CYP3A4 Supersomes with MDZ and ITZ, up to 40% of the inhibitor pool was depleted during the 2-min incubation period, and OH-ITZ could be quantified in all incubation products. For reaction mixtures with relatively high initial ITZ concentrations, keto-ITZ could be detected as well. Depletion of OH-ITZ during MDZ incubation was significantly less than that of ITZ, 5 to 10%, and was observed only at the low initial OH-ITZ concentrations. The measured concentrations of OH-ITZ and keto-ITZ as metabolites were used to evaluate the possible contribution of these metabolites to the inhibition of midazolam hydroxylation. OH-ITZ was present at levels 10 times lower than the ITZ concentration when ITZ was used as an inhibitor. At the highest ITZ concentration used, OH-ITZ concentrations rose to concentrations equal to its K_i at 2 min, whereas in the incubation with ITZ at 280 nM, OH-ITZ concentrations at 2 min were 0.5 times its K_i. At the lowest ITZ concentration, OH-ITZ concentrations were approximately 10-fold below its measured K_i. When OH-ITZ was used as the inhibitor, keto-ITZ concentrations were 4 to 10 times lower than those of OH-ITZ. Based on these results, it is unlikely that OH-ITZ and keto-ITZ contributed by a reversible mechanism to CYP3A4 inhibition following incubation with ITZ under the in vitro conditions used. However, because of the

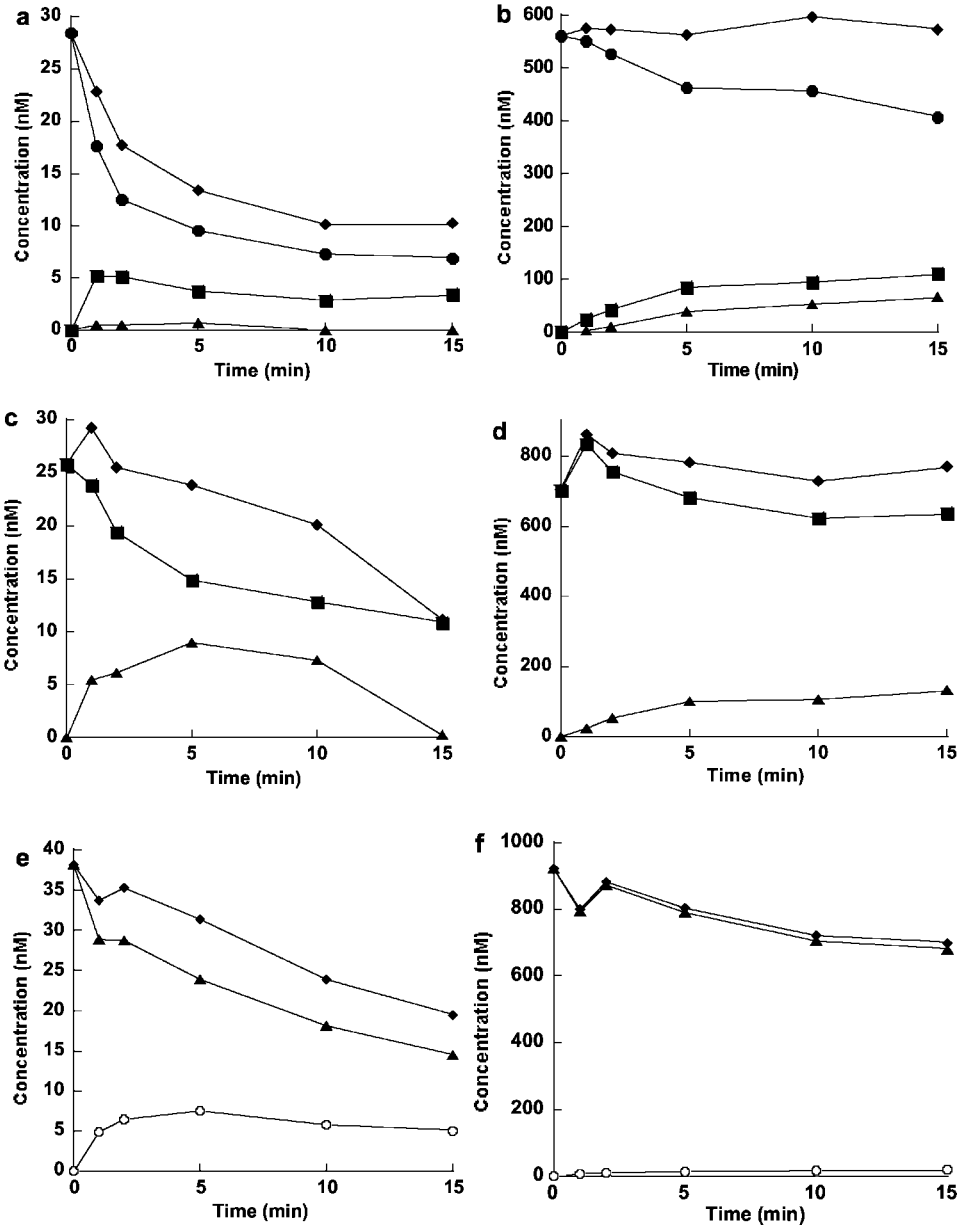

FIG. 5. Concentrations of ITZ, OH-ITZ, and keto-ITZ in incubations of ITZ (a and b), OH-ITZ (c and d), and keto-ITZ (e and f) with heterologously expressed CYP3A4. ITZ concentrations were 28 nM (a) and 580 nM (b), OH-ITZ concentrations were 25 nM (c) and 337 nM (d), and keto-ITZ concentrations were 37 nM (e) and 923 nM (f). Incubation conditions were as described under *Materials and Methods*. ◆, total calculated concentration; ●, measured ITZ; ■, measured OH-ITZ; ▲, measured keto-ITZ; and ○, measured ND-ITZ.

partial depletion of ITZ at the lowest inhibitor concentrations, we cannot rule out a possible contribution from unknown ITZ metabolites to the overall inhibitory effect. It is also possible that there could be slowly reversible or irreversible CYP3A4 inhibition following incubation with ITZ, OH-ITZ, keto-ITZ, or ND-ITZ from the production of relatively small amounts of an unknown downstream ITZ metabolite(s).

The inhibitory potency of ITZ, OH-ITZ, keto-ITZ, and ND-ITZ was confirmed in experiments with pooled human liver microsomes. Figure 8 shows a plot of the inhibitor concentration versus percentage inhibition. All three compounds gave a maximum inhibition of >90% at the highest nominal concentration tested (1 μM for all compounds except ND-ITZ, which was 650 nM). At the lowest nominal inhibitor concentration, a small but consistent activation of CYP3A4 was observed. The IC_{50} values that were obtained are shown in Table 2. Interestingly, ND-ITZ was a more potent inhibitor of CYP3A4 in human liver microsomes than any of the other tested compounds, which had equivalent inhibitory potencies. ITZ and OH-ITZ depletion was less than that seen in experiments with CYP3A4 Supersomes. Only 5% of ITZ was depleted at the highest concentration used, and 25% of ITZ was depleted at the lowest concentration. In addition, there was no measurable depletion of OH-ITZ, keto-ITZ, or ND-ITZ under the liver microsomal incubation conditions involved. This difference between the Supersome and human liver microsome experiments is attributed to the lower amount of active CYP3A4 available in microsomal incubations.

Effect of Nonspecific Microsomal Binding on Inhibition Parameters. Nonspecific protein binding of ITZ, OH-ITZ, keto-ITZ, and ND-ITZ was measured in Supersomes and liver microsomes. All of the test compounds were bound extensively, even at the low

TABLE 1

Kinetic parameters for cDNA-expressed CYP3A4 (Supersomes)-mediated metabolism of ITZ, OH-ITZ, and keto-ITZ

	K_m ± S.D.	f_u ± S.D.	$K_{m,u}$	$k_{dep[S]\to 0}$ ± S.D.	V_{max}	$CL_{int,u}$
	nM	*%*	*nM*	*1/min*	*pmol/min/nmol 3A4*	*ml/min/nmol CYP3A4*
ITZ	44.4 ± 11.1	8.8 ± 3.2	3.9	0.69 ± 0.07	270	69.3
OH-ITZ	71.7 ± 37.5	38 ± 20	27	0.33 ± 0.06	543	19.8
keto-ITZ	17.9 ± 8.8	9.2 ± 4.9	1.4	0.63 ± 0.18	86.9	62.5

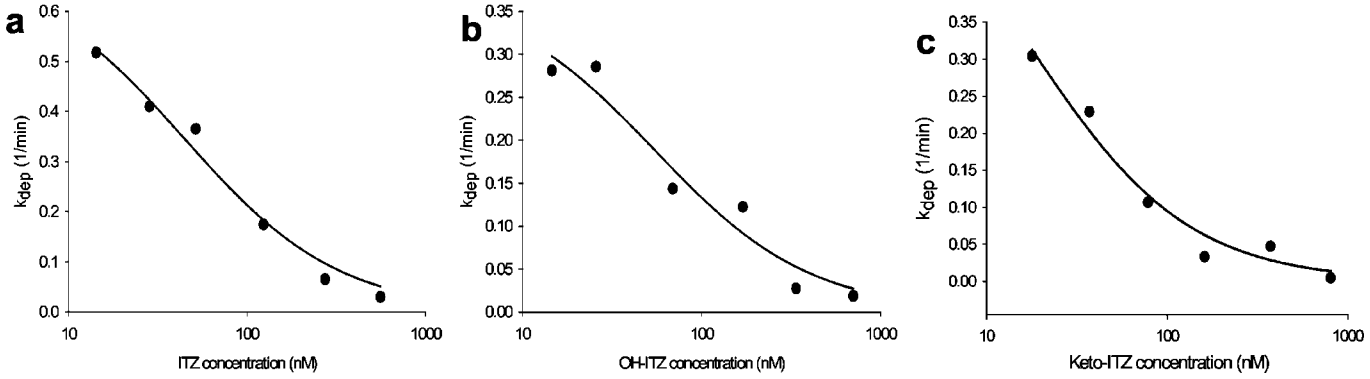

FIG. 6. Concentration versus first-order depletion rate constant (k_{dep}) plots and determination of Michaelis constants (with data nonlinearly fitted to eq. 5) for ITZ (a), OH-ITZ (b), and keto-ITZ (c), using the substrate depletion approach. Depletion rate constant for each substrate concentration was obtained as described under *Materials and Methods* using a linear fit of log percent remaining versus time plots.

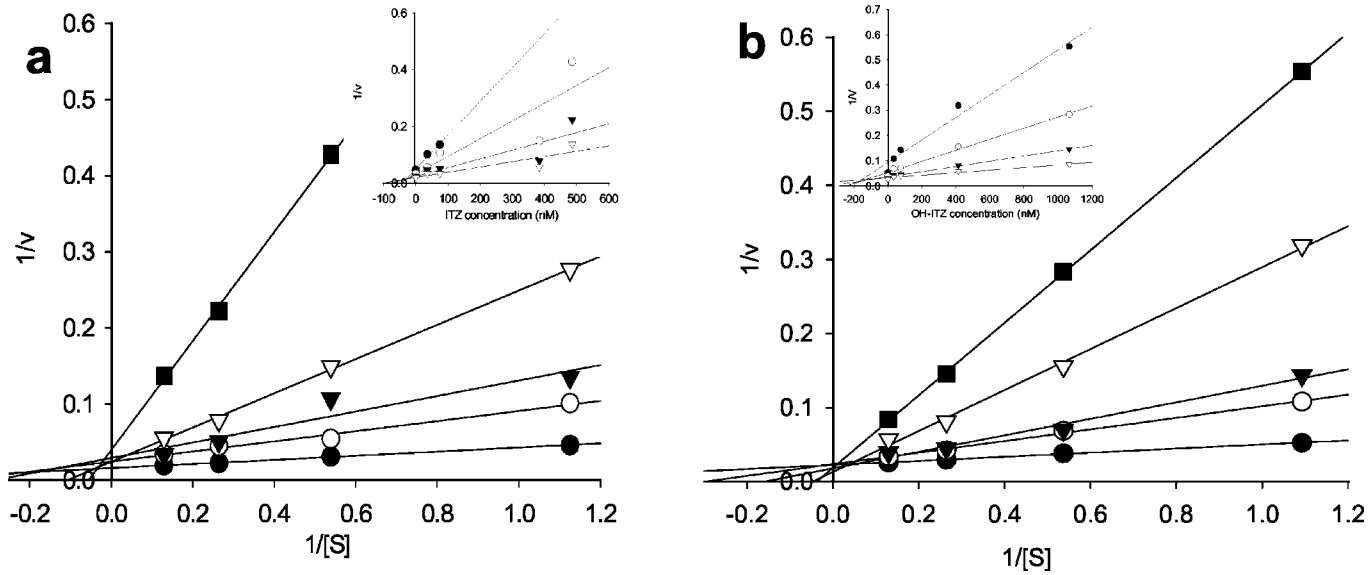

FIG. 7. Lineweaver-Burk plots for the inhibition of CYP3A4-mediated formation of 1-OH-midazolam by ITZ (a) and OH-ITZ (b). Insets show the corresponding Dixon plots.

protein concentrations of 0.025 to 0.087 mg/ml that were used. The unbound fraction of the test compounds was between 10 and 20% with the exception of OH-ITZ in Supersomes (38%) and ND-ITZ in microsomes (2.6%) (Tables 1 and 2), and the bound fraction appeared to be independent of the nominal inhibitor concentration (data not shown). Accordingly, the extensive protein binding had a significant effect on the observed K_m and K_i values and must be taken into account when in vitro-to-in vivo predictions are made. Also, the high lipophilicity of ITZ and its metabolites, their poor solubility in aqueous buffers, high protein binding, and low enzymatically relevant nominal concentrations make it extremely difficult to estimate the free fraction for ITZ and its metabolites accurately.

Discussion

Clinical evidence suggests that ITZ is a substrate of CYP3A4. The results of this study confirmed that OH-ITZ is generated from ITZ by CYP3A4. In addition, it was discovered that CYP3A4 further catalyzes the conversion of OH-ITZ to the corresponding ketone, keto-ITZ, and also catalyzes the dealkylation of the keto-ITZ and possibly ITZ and OH-ITZ, to generate ND-ITZ. These sequential oxidations may occur via two different mechanisms as suggested previously for testosterone and levo-α-acetylmethadol (Sugiyama et al., 1994; Oda and Kharasch, 2001). Either the primary metabolite-enzyme complex, OH-ITZ-CYP3A4, is activated and converted to the secondary metabolite, keto-ITZ before OH-ITZ is released from the enzyme, or

TABLE 2

Kinetic parameters for CYP3A4 inhibition by ITZ and its metabolites OH-ITZ, keto-ITZ, and ND-ITZ

K_i values were calculated from experiments with heterologously expressed CYP3A4 Supersomes, and IC_{50} values were determined from inhibition of midazolam hydroxylation in pooled human liver microsomes. The 95% confidence interval for the parameter estimates is presented in brackets.

	K_i	$K_{i,u}$	IC_{50} ± S.E.	f_u ± S.D.	$IC_{50,u}$
	nM		*nM*	*%*	*nM*
ITZ	15.7	1.3	29 ± 10 [0–58]	19.6 ± 9.2	6.1
OH-ITZ	37.8	14.4	37 ± 13 [5–70]	12.4 ± 6.8	4.6
keto-ITZ	NA	NA	53 ± 17 [10–97]	11.7 ± 4.2	7.0
ND-ITZ	NA	NA	17 ± 6.6 [0–34]	2.6 ± 1.2	0.44

NA, not available.

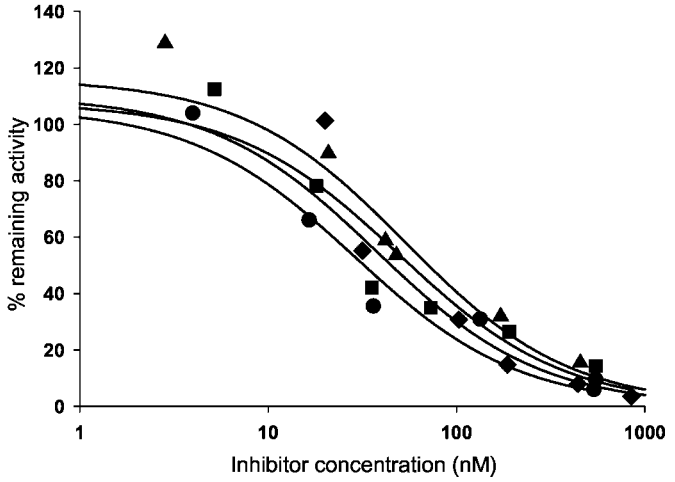

FIG. 8. Nominal inhibitor concentration versus percent remaining activity plots for ITZ, OH-ITZ, keto-ITZ, and ND-ITZ using pooled human liver microsomes and midazolam hydroxylation as a CYP3A4 probe reaction. ♦, ND-ITZ; ●, ITZ; ■, OH-ITZ; and ▲, keto-ITZ.

OH-ITZ is released from the enzyme and then reassociates with the enzyme to be oxidized to keto-ITZ. In the first scenario, the ratio of the keto-ITZ formation rate to the OH-ITZ formation rate will be constant with varying ITZ concentrations, whereas for the second scenario, the formation of keto-ITZ will eventually cease when enzyme becomes saturated with the initial substrate, ITZ (i.e., OH-ITZ will not reassociate after dissociation). Results from this study suggest something intermediate: keto-ITZ was detected both in incubations with ITZ at saturating concentrations (1 μM) and in incubations of high concentrations of ITZ and midazolam. This suggests that at least part of the keto-ITZ product must be generated from ITZ without dissociation of OH-ITZ from CYP3A4.

Two new metabolites of ITZ formed by CYP3A4 were identified in this study. Mass spectrometric and chromatographic data and comparison with authentic standards supports the identification of these metabolites as keto-ITZ and ND-ITZ. ND-ITZ has been previously reported as a urinary and fecally excreted metabolite of itraconazole in rats and dogs (Heykants et al., 1987). Since ITZ is not excreted unchanged into the urine and only a small fraction of the dose (5%) is excreted unchanged in the feces, the three metabolites described here may contribute significantly to the urinary recovery of ITZ. At present it is not known whether keto-ITZ and ND-ITZ circulate in plasma in vivo, but due to the sequential, partly nondissociative nature of ITZ metabolism by CYP3A4 to keto-ITZ via OH-ITZ, one could expect that significant amounts of keto-ITZ would be formed in vivo. However, the ketone metabolite may be rapidly reduced to the alcohol by reductase enzymes, resulting in a disproportionate accumulation of OH-ITZ as CYP3A4 activity is inhibited with multiple ITZ dosing. There is also the possibility of *N*-dealkylation of keto-ITZ by CYP3A4.

The biphasic elimination of ITZ observed at all nominal in vitro concentrations mimics the elimination profile observed in vivo. The biphasic elimination of ITZ in vivo has thus far been explained by distribution kinetics. However, it is unlikely that distribution accounts for the biphasic elimination in the expressed enzyme system. Recently, it was reported that the stereoisomers of ITZ have significantly different plasma concentrations (Breadmore and Thormann, 2003). Thus, stereoselective clearance of the four ITZ stereoisomers (two enantiomeric pairs) by CYP3A4 would be a plausible explanation for the biphasic elimination of total ITZ observed in our in vitro incubations and in vivo. A set of high clearance stereoisomers (pair of enantiomers) might account for the initial fast elimination phase and a set of low-clearance enantiomers attributing to the second slower elimination phase. Alternatively, the biphasic depletion of ITZ in vitro and in vivo could involve gradual loss of enzyme activity by time-dependant inactivation of the enzyme or inhibition of the enzyme by accumulating metabolites.

Results from a previous study by Yamano et al. (2001) suggest that ITZ does not cause irreversible time-dependent inactivation of CYP3A4 when incubated with human liver microsomes. However, this finding may be incubation condition-dependent, particularly in view of the apparent high affinity of downstream ITZ metabolites such as ND-ITZ for CYP3A4. It is possible that metabolism of ND-ITZ may eventually result in a metabolite-enzyme complex that is so stable (toward further metabolism and dissociation) as to effectively preclude any productive metabolism of other CYP3A4 substrates. Preliminary experiments provided us with no convincing evidence that classical mechanism-based inhibition occurs, but more careful experimentation is needed to evaluate this mechanistic possibility.

ITZ exhibits a disproportional increase in AUC with increasing single oral doses and a time-dependent reduction in oral clearance with multiple dosing (Hardin et al., 1988; Heykants et al., 1989; Haria et al., 1996). In addition, ITZ bioavailability is dose-dependent (Schäfer-Körting, 1993), and ITZ elimination was found to follow Michaelis-Menten kinetics in vivo (Barone et al., 1993). Given our in vitro findings, concentration-, dose-, and time-dependent kinetic nonlinearity may be a consequence of saturation of intestinal and hepatic CYP3A4 by ITZ metabolites, in addition to the parent drug.

A number of investigators have evaluated the inhibitory potency of ITZ toward CYP3A4 in human liver microsomes. The probe substrates have included cyclosporine (Back and Tjia, 1991), midazolam (von Moltke et al., 1996; Wang et al., 1999), diazepam (Tran et al., 2002), and simvastatin (Ishigam et al., 2001). Using midazolam as a probe, two different investigators obtained a 10-fold difference in the K_i values for ITZ, 2300 nM (Wang et al., 1999) and 270 nM (von Moltke et al., 1996). However, the microsomal protein content used in the studies was 0.25 mg/ml. Using cyclosporine as a probe and 0.15 mg/ml microsomal protein, an ITZ K_i of 700 nM was reported (Back and Tjia, 1991). More recently, Ishigam et al. (2001) obtained a range of K_i values of 27 to 93 nM for ITZ using simvastatin as a probe and 0.04 mg/ml microsomal protein. These studies show a trend toward a lower K_i measurement with decreasing protein concentrations, reflective of significant nonspecific microsomal protein binding and possibly inhibitor depletion. Indeed, the study by Tran et al. (2002) showed a consistent decrease in the inhibitory potency of ITZ with increasing

protein concentrations, supporting the theory that nonspecific microsomal binding affects the in vitro K_i of ITZ. The study by Ishigam et al. (2001) also measured the unbound liver microsomal K_i for ITZ, which was 1.4 to 4.7 nM. The results presented here for ITZ (K_i 15.7 nM and $K_{i,u}$ 1.3 nM), using expressed CYP3A4, are similar to their data, although slightly lower in magnitude.

Previous investigators have also evaluated the inhibitory potency of OH-ITZ toward CYP3A4 in human liver microsomes using MDZ, triazolam or diazepam as a substrate probe (von Moltke et al., 1998; Wang et al., 1999; Tran et al., 2002). For two of the studies, (von Moltke et al., 1998; Wang et al., 1999), OH-ITZ was a slightly less potent inhibitor of CYP3A4 than ITZ (1.2- to 2.7 fold), and for the other (Tran et al., 2002) it was 2-fold more potent than ITZ. The reported K_i or IC_{50} values for OH-ITZ varied between 95 - 6300 nM. These parameter values illustrate the substantial affinity of OH-ITZ for CYP3A4, but do not adequately explain the observed in vivo inhibitory effect of ITZ after consideration of expected unbound circulating OH-ITZ plasma concentrations. In contrast, the unbound K_i and IC_{50} of OH-ITZ determined in this study are at least 7-fold lower than previously reported parameter values and make a much stronger case for a significant contribution from OH-ITZ to the in vivo inhibitory effect.

In addition to OH-ITZ, which is known to circulate at higher concentrations than ITZ in plasma (Heykants et al., 1989; Barone et al., 1993; Poirier and Cheymol, 1998), the new metabolites identified in this study, keto-ITZ and ND-ITZ, may contribute to the increased inhibition of CYP3A4 by ITZ with longer therapy. Some investigators have observed an unusually persistent inhibition of CYP3A4-mediated metabolism of tacrolimus and cyclosporine by ITZ after cessation of ITZ administration (Trenk et al., 1987; Cervelli and Russ, 2003). This prolonged inhibitory effect, which exceeds in duration four half-lives of ITZ, could be explained by circulating metabolites of ITZ that have half-lives that exceed that of the parent drug, or slow dissociation of an inhibitory metabolite-enzyme complex. The fact that ND-ITZ was the most potent inhibitor of the tested compounds in this study, and has been detected as a urinary metabolite of ITZ in humans and animals, would support the hypothesis that this metabolite contributes significantly to the persistent inhibition of CYP3A4 in vivo.

ITZ is a triazole antifungal agent that is traditionally believed to bind to the fungal P450 by coordinating the heme via the triazole ring nitrogen. This has also been the supposed mechanism for CYP3A4 inhibition. However, the close agreement of the determined $K_{i,u}$ and $K_{m,u}$ values suggests an alternative hypothesis. Coordination to the heme-iron of CYP3A4 by ITZ is not a prerequisite for inhibition, but instead, inhibition of CYP3A4 may occur due to its metabolism via this enzyme at the opposite end of the substrate/inhibitor molecule. (This assumes that metabolism of ITZ to OH-ITZ cannot occur if the triazole nitrogen is coordinated to the heme-iron.) Further experiments are underway to explore this possibility.

Results from this investigation do not exclude the possibility that there is active, concentrative uptake of ITZ into human hepatocytes and that this process contributes to the apparent potency of ITZ as an inhibitor of CYP3A4 in vivo. Data to support this mechanistic explanation come from rat liver experiments, and confirmation with human hepatocytes is needed. Ultimately, the profound effects of ITZ therapy on CYP3A-catalyzed drug clearance may be multifactorial.

In conclusion, this study has shown that ITZ and its subsequent sequential metabolites (OH-ITZ, keto-ITZ, and ND-ITZ) are all high-affinity ligands of CYP3A4, and they undergo metabolism by CYP3A4. These metabolites may contribute to CYP3A4 inhibition in vivo following ITZ therapy. The results of this study also provide insight into the reasons for underprediction of CYP3A4 inhibition by ITZ in vivo from in vitro K_i data and suggest that nonspecific protein binding, accumulation of inhibitory metabolites, and inhibitor depletion can contribute to mispredictions.

References

Back DJ and Tjia JF (1991) Comparative effects of the antimycotic drugs ketoconazole, fluconazole, itraconazole and terbinafine on the metabolism of cyclosporin by human liver microsomes. *Br J Clin Pharmacol* **32:**624–626.

Backman JT, Kivisto KT, Olkkola KT, and Neuvonen PJ (1998) The area under the plasma concentration-time curve for oral midazolam is 400-fold larger during treatment with itraconazole than with rifampicin. *Eur J Clin Pharmacol* **54:**53–58.

Banerjee R, Leaver N, Lyster H, and Banner NR (2001) Coadministration of itraconazole and tacrolimus after thoracic organ transplantation. *Transplant Proc* **33:**1600–1602.

Barone JA, Koh JG, Bierman RH, Colaizzi JL, Swanson KA, Gaffar MC, Moskovitz BL, Mechlinski W, and Van de Velde V (1993) Food interaction and steady-state pharmacokinetics of itraconazole capsules in healthy male volunteers. *Antimicrob Agents Chemother* **37:**778–784.

Bonay M, Jonville-Bera AP, Diot P, Lemarie E, Lavandier M, and Autret E (1993) Possible interaction between phenobarbital, carbamazepine and itraconazole. *Drug Safety* **9:**309–311.

Breadmore MC and Thormann W (2003) Capillary electrophoresis evidence for the stereoselective metabolism of itraconazole in man. *Electrophoresis* **24:**2588–2597.

Cervelli MJ and Russ GR (2003) Itraconazole-tacrolimus drug interaction. *Ther Drug Monit* **25:**483–484.

Ducharme MP, Slaughter RL, Warbasse LH, Chandrasekar PH, Van de Velde V, Mannens G, and Edwards DJ (1995) Itraconazole and hydroxyitraconazole serum concentrations are reduced more than tenfold by phenytoin. *Clin Pharmacol Ther* **58:**617–624.

Florea NR, Capitano B, Nightingale CH, Hull D, Leitz GJ, and Nicolau DP (2003) Beneficial pharmacokinetic interaction between cyclosporine and itraconazole in renal transplant recipients. *Transplant Proc* **35:**2873–2877.

Hardin TC, Graybill JR, Fetchick R, Woestenborghs R, Rinaldi MG, and Kuhn JG (1988) Pharmacokinetics of itraconazole following oral administration to normal volunteers. *Antimicrob Agents Chemother* **32:**1310–1313.

Haria M, Bryson HM, and Goa KL (1996) Itraconazole. A reappraisal of its pharmacological properties and therapeutic use in the management of superficial fungal infections. *Drugs* **51:**585–620.

Heeres J, Backx LJ, and Van Cutsem J (1984) Antimycotic azoles. 7. Synthesis and antifungal properties of a series of novel triazol-3-ones. *J Med Chem* **27:**894–900.

Heykants J, Michielis M, Meuldermans W, Monbaliu J, Lavrijsen K, Van Peer A, Levron JC, Woestenborghs R, and Cauwenbergh G (1987) The pharmacokinetics of itraconazole in animals and man: an overview, in *Recent Trends in the Discovery, Development and Evaluation of Antifungal Agents* (Fromtling RA ed), pp 223–249, J.R. Prous Science Publishers, Barcelona.

Heykants J, Van Peer A, Van de Velde V, Van Rooy P, Meuldermans W, Lavrijsen K, Woestenborghs R, Van Cutsem J, and Cauwenbergh G (1989) The clinical pharmacokinetics of itraconazole: an overview. *Mycoses* **32 (Suppl 1):**67–87.

Ishigam M, Uchiyama M, Kondo T, Iwabuchi H, Inoue S, Takasaki W, Ikeda T, Komai T, Ito K, and Sugiyama Y (2001) Inhibition of in vitro metabolism of simvastatin by itraconazole in humans and prediction of in vivo drug-drug interactions. *Pharm Res (NY)* **18:**622–631.

Kivistö KT, Lamberg TS, and Neuvonen PJ (1999) Interactions of buspirone with itraconazole and rifampicin: effects on the pharmacokinetics of the active 1-(2-pyrimidinyl)-piperazine metabolite of buspirone. *Pharmacol Toxicol* **84:**94–97.

Kwan JT, Foxall PJ, Davidson DG, Bending MR, and Eisinger AJ (1987) Interaction of cyclosporin and itraconazole. *Lancet* **2:**282.

Lebrun-Vignes B, Archer VC, Diquet B, Levron JC, Chosidow O, Puech AJ, and Warot D (2001) Effect of itraconazole on the pharmacokinetics of prednisolone and methylprednisolone and cortisol secretion in healthy subjects. *Br J Clin Pharmacol* **51:**443–450.

Lin YS, Dowling AL, Quigley SD, Farin FM, Zhang J, Lamba J, Schuetz EG, and Thummel KE (2002) Co-regulation of CYP3A4 and CYP3A5 and contribution to hepatic and intestinal midazolam metabolism. *Mol Pharmacol* **62:**162–172.

Lowry OH, Rosebrough NJ, Farr AL, and Randall RJ (1951) Protein measurement with the Folin phenol reagent. *J Biol Chem* **193:**265–275.

Mahnke CB, Sutton RM, Venkataramanan R, Michaels M, Kurland G, Boyle GJ, Law YM, Miller SA, Pigula FA, Gandhi S, and Webber SA (2003) Tacrolimus dosage requirements after initiation of azole antifungal therapy in pediatric thoracic organ transplantation. *Pediatr Transplant* **7:**474–478.

Neuvonen PJ and Jalava KM (1996) Itraconazole drastically increases plasma concentrations of lovastatin and lovastatin acid. *Clin Pharmacol Ther* **60:**54–61.

Neuvonen PJ, Kantola T, and Kivisto KT (1998) Simvastatin but not pravastatin is very susceptible to interaction with the CYP3A4 inhibitor itraconazole. *Clin Pharmacol Ther* **63:**332–341.

Obach RS and Reed-Hagen AE (2002) Measurement of Michaelis constants for cytochrome P450-mediated biotransformation reactions using a substrate depletion approach. *Drug Metab Dispos* **30:**831–837.

Oda Y and Kharasch ED (2001) Metabolism of levo-alpha-acetylmethadol (LAAM) by human liver cytochrome P450: involvement of CYP3A4 characterized by atypical kinetics with two binding sites. *J Pharmacol Exp Ther* **297:**410–422.

Olkkola KT, Ahonen J, and Neuvonen PJ (1996) The effect of systemic antimycotics, itraconazole and fluconazole, on the pharmacokinetics and pharmacodynamics of intravenous and oral midazolam. *Anesth Analg* **82:**511–516.

Poirier JM and Cheymol G (1998) Optimisation of itraconazole therapy using target drug concentrations. *Clin Pharmacokinet* **35:**461–473.

Schäfer-Körting M (1993) Pharmacokinetic optimisation of oral antifungal therapy. *Clin Pharmacokinet* **25:**329–341.

Sugiyama K, Nagata K, Gillette JR, and Darbyshire JF (1994) Theoretical kinetics of sequential metabolism in vitro. Study of the formation of 16 alpha-hydroxyandrostenedione from testosterone by purified rat P450 2C11. *Drug Metab Dispos* **22:**584–591.

Tidwell TT (1990) Oxidation of alcohols to carbonyl compounds via alkoxysulfonium ylides: the Moffat, Swern and related oxidations. *Org React* **39:**297–572.
Tran TH, Von Moltke LL, Venkatakrishnan K, Granda BW, Gibbs MA, Obach RS, Harmatz JS, and Greenblatt DJ (2002) Microsomal protein concentration modifies the apparent inhibitory potency of CYP3A inhibitors. *Drug Metab Dispos* **30:**1441–1445.
Trenk D, Brett W, Jahnchen E, and Birnbaum D (1987) Time course of cyclosporin/itraconazole interaction. *Lancet* **2:**1335–1336.
Tucker RM, Denning DW, Hanson LH, Rinaldi MG, Graybill JR, Sharkey PK, Pappagianis D, and Stevens DA (1992) Interaction of azoles with rifampin, phenytoin and carbamazepine: in vitro and clinical observations. *Clin Infect Dis* **14:**165–174.
von Moltke LL, Greenblatt DJ, Duan SX, Harmatz JS, and Shader RI (1998) Inhibition of triazolam hydroxylation by ketoconazole, itraconazole, hydroxyitraconazole and fluconazole in-vitro. *Pharm Pharmacol Commun* **4:**443–445.
von Moltke LL, Greenblatt DJ, Schmider J, Duan SX, Wright CE, Harmatz JS, and Shader RI (1996) Midazolam hydroxylation by human liver microsomes in vitro: inhibition by fluoxetine, norfluoxetine and by azole antifungal agents. *J Clin Pharmacol* **36:**783–791.
Wang JS, Wen X, Backman JT, Taavitsainen P, Neuvonen PJ, and Kivisto KT (1999) Midazolam alpha-hydroxylation by human liver microsomes in vitro: inhibition by calcium channel blockers, itraconazole and ketoconazole. *Pharmacol Toxicol* **85:**157–161.
Weerawarna SA, Guha-Biswas M, and Nelson WL (1991) Benzofurans. Improved synthesis of bufuralol, 7-ethyl-2-(2-tert-butylamino-1-hydroxyethyl)benzofuran and 1″-oxobufuralol, 7-acetyl-2-(2-tert-butylamino-1-hydroxyethyl)benzofuran. *J Heterocycl Chem* **28:**1395–1403.
Yamano K, Yamamoto K, Katashima M, Kotaki H, Takedomi S, Matsuo H, Ohtani H, Sawada Y, and Iga T (2001) Prediction of midazolam-CYP3A inhibitors interaction in the human liver from in vivo/in vitro absorption, distribution and metabolism data. *Drug Metab Dispos* **29:**443–452.

Address correspondence to: Kenneth E. Thummel, University of Washington, Department of Pharmaceutics, H272 Health Sciences Building, Box 357610, Seattle, WA 98195-7610. E-mail: thummel@u.washington.edu